PIBB 生物化学与生物物理进展
Progress in Biochemistry and Biophysics
2025, 52(8): 2103~2116
www.pibb.ac.cn

Junctophilin-2 MORN-Helix Domain: Structural Basis for Membrane Binding and Hypertrophic Cardiomyopathy-associated Mutations*

WANG Jing-Xin[1)], LI Zhi-Wei[1)], LIU Wei[2)], ZHANG Wen-Qing[1)], LI Jian-Chao[1)**]

([1)]*Innovation Centre of Ministry of Education for Development and Diseases, School of Medicine, South China University of Technology, Guangzhou* 510006, China;

[2)]*Shenzhen Key Laboratory for Neuronal Structural Biology, Biomedical Research Institute, Shenzhen Peking University-The Hong Kong University of Science and Technology Medical Center, Shenzhen* 518036, China)

Graphical abstract

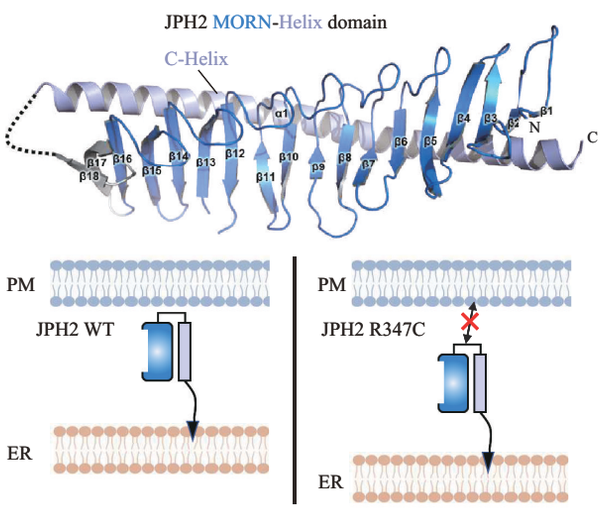

Abstract **Objective** Junctophilin-2 (JPH2) is an essential structural protein that maintains junctional membrane complexes (JMCs) in cardiomyocytes by tethering the plasma membrane to the sarcoplasmic reticulum, thereby facilitating excitation-contraction (E-C) coupling. Mutations in JPH2 have been associated with hypertrophic cardiomyopathy (HCM), but the molecular mechanisms governing its membrane-binding properties and the functional relevance of its membrane occupation and recognition nexus (MORN) repeat motifs remain incompletely understood. This study aimed to elucidate the structural basis of JPH2 membrane association and its implications for HCM pathogenesis. **Methods** A recombinant N-terminal fragment of mouse JPH2 (residues 1-440), encompassing the MORN repeats and an adjacent helical region, was purified under near-physiological buffer conditions. X-ray crystallography was employed to determine the structure of the JPH2 MORN-Helix domain. Sequence conservation analysis across species and junctophilin isoforms was performed to assess the evolutionary conservation of key structural features. Functional

* This work was supported by a grant from The National Natural Science Foundation of China (32271270).

** Corresponding author.
Tel: 86-15919631934, E-mail: lijch@scut.edu.cn

Received: April 25, 2025 Accepted: June 2, 2025

membrane-binding assays were conducted using liposome co-sedimentation and cell-based localization studies in COS7 and HeLa cells. In addition, site-directed mutagenesis targeting positively charged residues and known HCM-associated mutations, including R347C, was used to evaluate their effects on membrane interaction and subcellular localization. **Results** The crystal structure of the mouse JPH2 MORN-Helix domain was resolved at 2.6 Å, revealing a compact, elongated architecture consisting of multiple tandem MORN motifs arranged in a curved configuration, forming a continuous hydrophobic core stabilized by alternating aromatic residues. A C-terminal α-helix further reinforced structural integrity. Conservation analysis identified the inner groove of the MORN array as a highly conserved surface, suggesting its role as a protein-binding interface. A flexible linker segment enriched in positively charged residues, located adjacent to the MORN motifs, was found to mediate direct electrostatic interactions with negatively charged phospholipid membranes. Functional assays demonstrated that mutation of these basic residues impaired membrane association, while the HCM-linked R347C mutation completely abolished membrane localization in cellular assays, despite preserving the overall MORN-Helix fold in structural modeling. **Conclusion** This study provides structural insight into the membrane-binding mechanism of the cardiomyocyte-specific protein JPH2, highlighting the dual roles of its MORN-Helix domain in membrane anchoring and protein interactions. The findings clarify the structural basis for membrane targeting *via* a positively charged linker and demonstrate that disruption of this interaction—such as that caused by the R347C mutation—likely contributes to HCM pathogenesis. These results not only enhance current understanding of JPH2 function in cardiac E-C coupling but also offer a structural framework for future investigations into the assembly and regulation of JMCs in both physiological and disease contexts.

Key words Junctophilin-2, MORN repeats, membrane binding, hypertrophic cardiomyopathy

DOI：10.16476/j.pibb.2025.0183 **CSTR**：32369.14.pibb.20250183

Junctophilins (JPHs) are a family of membrane-associated proteins critical for forming junctional membrane complexes (JMCs) in excitable tissues, such as skeletal and cardiac muscle and neurons[1-3]. These complexes physically link the plasma membrane to the endoplasmic or sarcoplasmic reticulum (ER/SR), facilitating calcium signaling and ion channel regulation essential for muscle contraction and neuronal activity[4-6]. The JPH family, comprising four isoforms (JPH1-4), is predominantly expressed in muscle cells and neurons, where they maintain the structural and functional integrity of JMCs[7-9]. Recent reviews have highlighted the multifaceted roles of JPHs in cellular signaling, tissue development, and disease pathogenesis, with implications for neurodegenerative disorders and heart failure[10-12]. Despite these advances, the precise molecular mechanisms governing JPH-mediated membrane interactions and their contributions to cellular architecture remain incompletely understood.

JPHs interact with cellular membranes through specialized protein motifs, notably the membrane occupation and recognition nexus (MORN) repeats, which are hypothesized to mediate membrane association[1]. Additionally, MORN repeats can function as protein-interacting modules, binding to ion channels such as L-type calcium channels (CaV), which are essential for assembling membrane junctions that facilitate efficient intracellular communication, especially in calcium signaling. In cardiac and skeletal muscle, JPHs stabilize triad junctions, maintaining the structural integrity of the ER/SR and supporting the calcium release required for excitation-contraction coupling[13-14]. However, the mechanisms by which MORN repeats of JPHs coordinate their membrane binding and protein interactions remain largely unknown.

MORN repeats, typically comprising 23−26 residues with the first 14 following the consensus sequence YxGxWxxGxxxGxG, often occur in tandem and form a β-sheet structure[15]. Originally named for their proposed role in membrane recognition and interaction, MORN repeats have since been identified in a wide range of proteins, including MORN1−5, SETD7/9, and plant PIPK, suggesting that this motif plays a critical role in diverse cellular processes[2, 15]. However, conflicting reports on the membrane-binding capacity of MORN repeats, with some studies indicating weak or negligible phospholipid interactions, underscore the need for further investigation. The conservation of the MORN repeats of JPHs implies a broad biological significance, but isolating pure, soluble MORN repeats containing fragments that retain functional properties is technically demanding. These challenges complicate mechanistic insights into their physiological roles,

particularly in resolving the debate over their membrane-binding specificity.

In this study, by optimizing constructs, purification strategies, and buffer conditions, we successfully obtained a highly purified, soluble N-terminal fragment of mouse JPH2 (residues 1−440), enabling us to investigate its membrane-binding properties and gain structural insights into its function. After removing the unstructured Joining region (residues 154−273), we determined the 2.6 Å crystal structure of the mouse JPH2 MORN-Helix domain (residues 1−153 and 274−421). The structure revealed a folding mechanism for the MORN repeats involving a unique core of alternating aromatic residues from each repeat stabilization by the C-terminal α-helix. This folding pattern aligns with our previous findings on MORN4, suggesting a conserved mechanism for structural stability. We demonstrated that the integrity of the MORN repeats and the C-terminal α-helix is sufficient for direct membrane binding, as shown by cell-based assays and *in vitro* liposome-binding assay. Furthermore, we identified a flexible linker segment containing positively charged residues critical for membrane association. Notably, the HCM-associated mutation R347C disrupts these interactions, providing novel insights into the molecular mechanisms underlying JPH-related diseases.

1 Methods

1.1 Constructs and protein purification

The cDNA encoding the mouse JPH2 N-terminal fragments (residues 1−440, NCBI accession code: NM_021566.2), mouse JPH1/JPH3 N-terminal fragments (residues 1−436/1−455, NCBI accession code: NM_020604.2/NM_020605.3) were PCR amplified from a mouse cDNA library. The MORN-Helix domain fragments (residues 1−153 and 274−421) was obtained by amplified the DNA fragments of mouse JPH2 NT by PCR, excluding the intervening linker region (residues 154−273) during cloning. All point mutations or deletion constructs were created by a PCR-based mutagenesis method. All of these constructs were cloned into a modified pETMBP.3C/pET32M.3C vector for protein expression in bacteria or a modified pTGFP vector for expression in COS7 cells.

All proteins were expressed in *Escherichia coli* BL21 or Rosetta. The N-terminal thioredoxin-His6-tagged proteins were purified with a Ni^{2+}-NTA Sepharose™ 6 Fast Flow column and followed by a Superdex-200 preparation grade size-exclusion chromatography. The purification tag was cleaved by protease 3C and the proteins were further purified by a step of ion-exchange chromatography or another cycle of size-exclusion chromatography in the final buffer containing 50 mmol/L Tris-HCl, pH 7.5 and 1 mmol/L DTT, with either 500 mmol/L NaCl, 1 mmol/L EDTA or 100 mmol/L $MgSO_4$ as required.

1.2 Size exclusion chromatography coupled with multiangle light scattering （SEC−MALS） assay

Protein samples (typically 200 μl at a concentration of 100 μmol/L) were injected into an ÄKTA-SEC system with a Superose™ 10/300 GL column (Cytiva) using the column buffer of 50 mmol/L Tris-HCl, pH 7.5 and 1 mmol/L DTT, with either 500 mmol/L NaCl, 1 mmol/L EDTA or 100 mmol/L $MgSO_4$ as required. The chromatography system was coupled to a static multi-angle light scattering system equipped with a 3-angle static light scattering detector (miniDAWN, Wyatt) and a differential refractive index detector (Optilab, Wyatt). The molecular masses were analyzed using the ASTRA 7 software (Wyatt).

1.3 Circular dichroism spectroscopy （CD） assay

The CD spectra of the proteins were acquired on a CD spectrometer (Applied Photophysics, UK) at 20℃. Spectra were recorded from 200 to 250 nm with three repeats using a quartz cell of 0.5 mm light path. The concentration of protein was 20 μmol/L in a buffer containing 50 mmol/L Tris-HCl (pH7.5), 500 mmol/L NaCl, 1 mmol/L EDTA and 1 mmol/L DTT. Thermal denaturation experiments of JPH2-NT (concentration at 20 μmol/L) were performed from 16−70℃ at a 2℃ stepped temperature ramping with a setting time of 30 s. The ellipticities at 208 nm were used to calculate the unfolded fraction and plotted as a function of temperature. The final curves are drawn by using GraphPad software. Melting point temperatures (T_m) were calculated by CDNN software.

1.4 Crystallography

The JPH2 MORN-Helix domain (residues 1−153 and 274−421) was crystallized using the hanging-drop vapor diffusion method at 16° C. Protein samples in 50 mmol/L Tris-HCl pH 7.5, 100 mmol/L $MgSO_4$, and 1 mmol/L DTT were mixed with a reservoir solution

containing 600 mmol/L magnesium sulfate hydrate and 100 mmol/L BIS-TRIS propane pH 7.0. For cryo-protection, crystals were quickly soaked in the reservoir solution supplemented with 10% (*v*/*v*) glycerol. X-ray diffraction data were collected at −173℃ on beamline BL19U1 at the Shanghai Synchrotron Radiation Facility. Data were processed and scaled automatically using the Aquarium pipeline[16].

The structure was determined by molecular replacement with Phaser[17], employing an AlphaFold2-generated model of mouse JPH2 as the search template[18]. The structure underwent iterative refinement, alternating between manual adjustments in Coot[19] and computational refinement in PHENIX[20]. Model quality was validated using MolProbity[21], with final refinement statistics reported in Table 1. Structural visualizations were created using PyMOL (http://www.pymol.org).

1.5 AlphaFold3−based predictions

The predicted structure of the MORN-Helix domain of JPH2 (amino acids 1−153, 275−421) was generated with AlphaFold3[22] on the AlphaFold Server (https://alphafoldserver.com).

1.6 Cell culture，cell imaging and data analysis

COS7 and HeLa cells (from ATCC) were cultured in DMEM supplemented with 10% FBS and 50−100 units of penicillin-streptomycin (P/S). Cultured COS7 cells were maintained at 37℃ with 5% CO_2. The cell lines were not further authenticated. Cells were tested negative for mycoplasma contamination by cytoplasmic DAPI staining.

Before transfection, 3×10^4−4×10^4 cells were plated on 6-well cell culture plates and allowed to adhere on 24 mm^2 1.5-1.8# glass coverslips overnight. After 8−16 h, cells were transiently transfected using jetOPTIMUS® DNA Transfection Reagent (Polyplus) following the manufacturer's instructions. Images were taken at 30−36 h.

All the images were acquired using a Zeiss LSM 800 laser-scanning confocal microscope, with a 63×2 NA oil-immersion objective and a pinhole setting of 1 Airy unit. Data were collected from three independent batches of cultures. At least 50−80 fluorescence-positive cells were counted for each group of experiments. All experiments were conducted in a double-blinded fashion. The data from each cell were quantified by Zeiss ZEN 3.3 (blue edition) and analyzed using ImageJ and GraphPad Prism 9.

1.7 Brain liposome sedimentation assay

Liposome stock was prepared by sonication of bovine lipid extracts (Folch Fraction I, Sigma) in assay buffers. Different concentrations of liposomes were incubated with the purified MBP-JPH2 NT or JPH2 MORN-Helix domain in the concentration of 5 μmol/L and in 50 mmol/L Tris, pH 7.5, 100 mmol/L $MgSO_4$ and 2 mmol/L DTT, buffer for 15 min at room temperature and then centrifuged at 200 000*g* for 30 min at 4℃ in a Beckman TLA100.1 rotor. The supernatants and the pellets were collected and subjected to SDS-PAGE analysis, and proteins were visualized by Coomassie blue staining.

1.8 Quantification and statistical analysis

Data of *in vitro* lipid binding assay were expressed as mean±SD. Data of cell imaging were expressed as scatter plot. The statistical analysis was performed using one-way ANOVA in the GraphPad Prism 9, *ns* not significant, **P*<0.05, ***P*<0.01, ****P*<0.001. All experiments related to cell cultures and COS7 imaging experiments were performed in double-blinded fashion.

2 Results

2.1 Purification of MBP−tagged JPH1−3 NT

All four JPH isoforms are predicted to contain 8 N-terminal MORN repeats (MORN1−8, with MORN6 and MORN7 separated by a long linker termed the "Joining region"), a subsequent α-helix (Helix), a divergent region, and a C-terminal transmembrane domain (TM) (Figure 1a)[1, 23-24]. Our previous study on MORN4 suggested that MORN repeats may interact with the adjacent α-helix to enhance stability. To investigate this in JPH2, we initially attempted to express and purify the mouse JPH2 N-terminal domain (NT, residues 1−440), encompassing the MORN repeats and Helix, using a thioredoxin (Trx) tag in *E. coli*. However, the Trx-fused JPH2 NT exhibited poor solubility (Figure 1b). To improve solubility and yield, we switched to a maltose-binding protein (MBP) fusion tag, which, as anticipated, significantly enhanced expression and solubility (Figure 1b). Following affinity chromatography, soluble MBP-tagged JPH2 NT was successfully obtained. However, size-exclusion

chromatography (SEC) revealed that in a standard buffer (100 mmol/L NaCl, 50 mmol/L Tris-HCl pH7.5, 1 mmol/L EDTA, 1 mmol/L DTT; hereafter “general buffer” or GB), JPH2 NT predominantly formed large aggregates (Figure 1c). To mitigate aggregation, we optimized the buffer composition. Addition of 10% glycerol to GB had no effect, but switching to phosphate-buffered saline (PBS) resulted in a fraction of the protein adopting a monomeric state. Hypothesizing that higher ionic strength might favor monomer formation, we increased the NaCl concentration in GB from 100 mmol/L to 500 mmol/L (denoted 500 GB). This adjustment markedly increased the proportion of monomeric JPH2 NT (Figure 1c, d). Using the same strategy, we successfully purified the NT domains of JPH1 and JPH3 (Figure 1e, f).

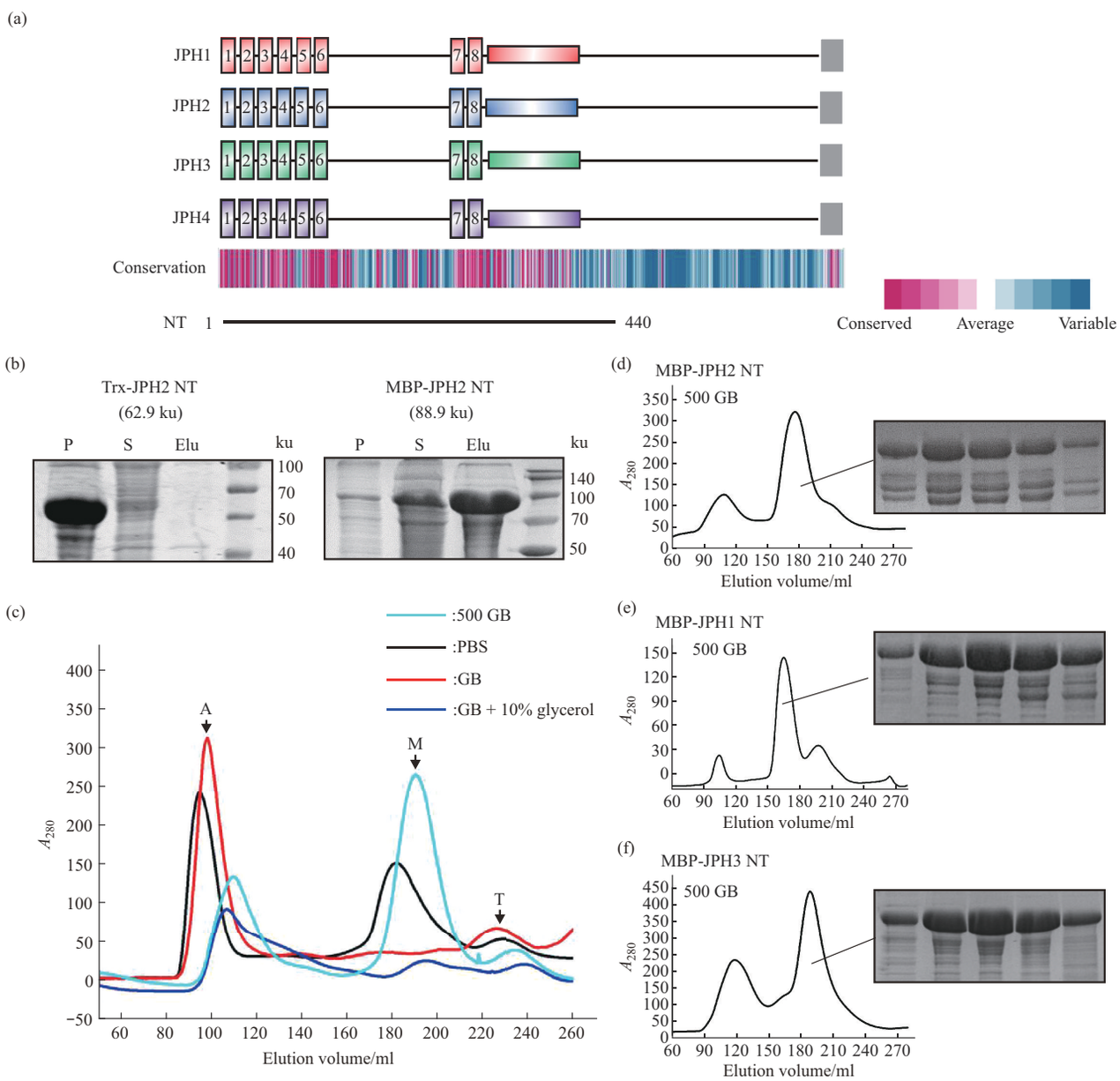

Fig. 1 High−salt buffer enhances soluble protein yield for JPH1−3 N−terminal fragments

(a) Domain organization of JPH1−4, illustrating key structural regions and conservation. (b) SDS-PAGE analysis of solubility for JPH2 N-terminal constructs (residues 1−440) fused to various tags following cell lysis. (c) Size-exclusion chromatography profiles of MBP-JPH2 NT (residues 1−440) on a Superdex 200 column under different buffer conditions: red curve (GB); black curve (PBS); cyan curve (500 GB); blue curve (GB+10% glycerol). Arrows indicate protein populations: A (aggregated), M (monomeric), T (MBP tag). (d−f) Gel-filtration chromatography profiles of MBP-fused JPH1−3 NT proteins on a Superdex 200 column, with corresponding SDS-PAGE results. All samples were eluted in 500 mmol/L NaCl, 50 mmol/L Tris-HCl pH 7.5, 1 mmol/L EDTA, and 1 mmol/L DTT. (d) JPH2-NT; (e) JPH1-NT; (f) JPH3-NT.

2.2 Improvement of protein quality with $MgSO_4$ buffer

Although the 500 GB buffer enabled purification of recombinant JPH2-NT protein, a significant fraction still formed aggregates. Additionally, the high ionic strength of 500 GB could disrupt protein-protein interactions in downstream studies. To address this, we further optimized the buffer composition. As divalent cations or sulfate ions can stabilize proteins, we replaced 500 mmol/L NaCl in 500 GB with 100 mmol/L $MgSO_4$ ($MgSO_4$ buffer) or 100 mmol/L $CaCl_2$ ($CaCl_2$ buffer). This modification markedly improved JPH2-NT stability. SEC coupled with multi-angle light scattering (SEC-MALS) revealed a symmetric elution peak with a molecular mass of 50.2 ku in $MgSO_4$ and 48.5 ku in $CaCl_2$, closely matching the theoretical molecular mass of 49.3 ku (Figure 2a, S1). SDS-PAGE analysis confirmed high purity, showing a single band (Figure 2b). Circular dichroism (CD) spectroscopy and CD-based thermal denaturation experiments further demonstrated that JPH2-NT was well-folded, with a T_m of 48°C (Figures 2c, d).

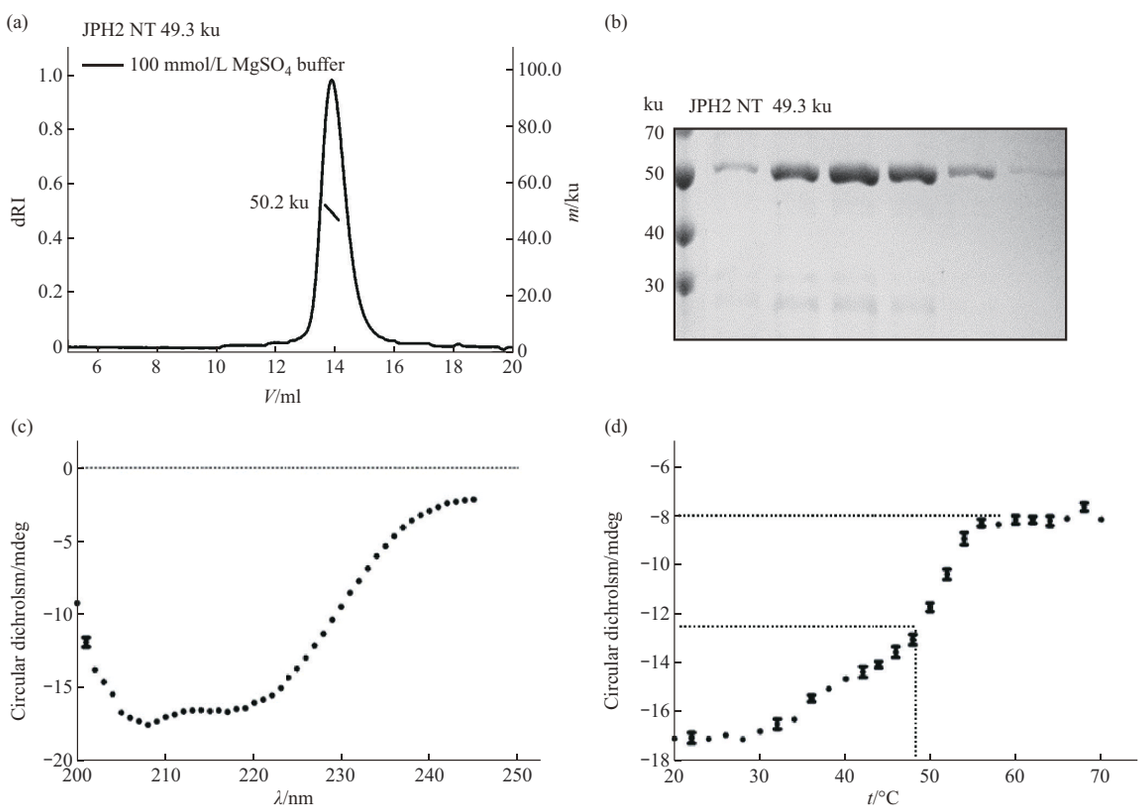

Fig. 2 $MgSO_4$ buffer enhances protein quality of JPH2 NT

(a) SEC-MALS analysis demonstrating that the JPH2 NT protein is monomeric in 50 mmol/L Tris-HCl pH 7.5, 100 mmol/L $MgSO_4$, 1 mmol/L DTT buffer. (b) SDS-PAGE analysis confirming high purity of MBP-fused JPH2 NT after purification. (c) CD spectrum of JPH2 NT, indicating a well-folded protein structure. (d) Thermal denaturation profile of JPH2 NT, plotting ellipticity at 208 nm against temperature. Melting temperature (T_m) was determined by fitting the curve to a sigmoid function.

2.3 Crystal structure of JPH2 MORN−Helix domain

To elucidate the structural basis of the JPH2 MORN-Helix domain, we pursued its crystal structure. As the Joining region (residues 154−273) is predicted to be intrinsically disordered (Figure 3a). We observed that the joining region exhibited relatively low sequence conservation when compared to the highly conserved MORN and Helix. Considering that poorly conserved, flexible, or intrinsically disordered regions often interfere with protein crystallization by increasing conformational heterogeneity and disrupting lattice packing, we chose to exclude this joining region during molecular

cloning to enhance the structural homogeneity and crystallization potential of the resulting MORN-Helix construct. By removing most of this linker, we generated a truncated construct (JPH2 MORN-Helix, residues 1−153 and 274−421) that yielded high-quality recombinant protein suitable for crystallization. We determined the crystal structure of JPH2 MORN-Helix at 2.6 Å resolution (Table 1).

Table 1 Statistics of X−ray crystallographic data collection and model refinement

Data collection	
Data sets	JPH2 MORN-Helix
Space group	$C222_1$
Wavelength/Å	0.979 18
Unit Cell Parameters/Å	a=69.48, b=73.31, c=139.97
	$\alpha=\beta=\gamma$=90°
Resolution range/Å	50−2.60 (2.72−2.60)
No. of unique reflections	11 353 (1 362)
Redundancy	12.4 (12.9)
I/σ	16.7 (2.4)
Completeness/%	99.8 (100)
R_{merge}/%[1)]	10.8 (123.8)
$CC_{1/2}$ (last resolution shell)[2)]	0.818
Structure refinement	
Resolution/Å	50−2.60 (2.86−2.60)
R_{cryst}[3)]/R_{free}[4)]/%	23.81/26.77 (32.21/34.42)
rmsd bonds (Å) / angles (°)	0.008/1.124
Average B factor (Å^2)[5)]	63.0
No. of atoms	
Protein atoms	1 998
Water	19
Ligands	5
No. of reflections	
Working set	10 744 (2 611)
Test set	584 (171)
Ramachandran plot regions[4)]	
Favored/%	95.31
Allowed/%	4.69
Outliers/%	0

Numbers in parentheses represent the value for the highest resolution shell. [1)]$R_{merge}=\Sigma|I_i - \langle I\rangle|/\Sigma I_i$, where I_i is the intensity of measured reflection and $\langle I\rangle$ is the mean intensity of all symmetry-related reflections. [2)]$CC_{1/2}$ were defined by Karplus and Diederichs[25]. [3)]$R_{cryst}=\Sigma||F_{calc}| - |F_{obs}||/\Sigma F_{obs}$, where F_{obs} and F_{calc} are observed and calculated structure factors. [4)]$R_{free}=\Sigma_T||F_{calc}| - |F_{obs}||/\Sigma F_{obs}$, where T is a test data set of about 5% of the total unique reflections randomly chosen and set aside prior to refinement. [5)]B factors and Ramachandran plot statistics are calculated using MOLPROBITY[21].

The JPH2 MORN-Helix structure adopts a skeletal framework, with a core comprising an 18-stranded antiparallel β-sheet (Figure 3b). This β-sheet exhibits a twisted configuration, with an approximately 90° angle between the first and last strands, forming a cradle-like structure with a concave inner surface and a convex outer surface. The concave side contains a narrow groove, ideally positioned for potential interactions with binding partners. Consistent with our previous findings on the MORN4 structure, the structure of JPH2 MORN repeats is stabilized by a unique folding core formed by the MORN repeats' aromatic residues. Specifically, aromatic residues at positions 1 (Y14, Y38, F60, Y82, Y106, Y129, Y285, Y308) and 5 (W18, W42, W64, W86, W110, F133, W289, W312) of the MORN repeats are arranged in an alternating (Figure 3c, S2), zipper-like pattern, forming a network of hydrophobic interactions that stabilize the core structure (Figure 3b).

On the convex side, a 65-residue α-helix runs parallel to the β-sheet, aligning with its twist and acting as a structural backbone (Figure 3d). This helix engages in extensive trans interactions with the β-sheet, mediated by hydrophobic contacts (*e.g.*, H26-I408, Y63/L72-A398, Y94-H387, Y118-I380, Y141-I373, Y320-K359), hydrogen bonds (*e.g.*, H26-E405, Y94-R384, Y118-K377), and a salt bridge (E332-R357). Additionally, conserved glycine residues at positions 3 and 14 in the MORN repeats (Figure 3c, S2), located on the backside of the β-sheet, contribute to these interactions. Their lack of side chains allows the helix to pack more closely against the β-sheet, enhancing structural stability.

To investigate the functional significance of the JPH2 MORN-Helix structure, we analyzed the sequence conservation of all JPH family members across species. The surface of the concave groove in the β-sheet is highly conserved, with two particularly conserved regions: one near the N-terminus and another near the C-terminus (Figure 3e). This conservation suggests that the groove, particularly these regions, likely serves as a common target protein binding site across the JPH family. Notably, recent structural biology studies revealed that a short peptide from the CaV1.1 C-terminus binds specifically to the N-terminal conserved region[23]. Furthermore, human genetic studies have identified the HCM-associated mutation E47A (corresponding to mouse E47) within this region. Analysis of the second conserved region near the C-terminus revealed additional HCM-related mutations—E121K, Y129D, and R300P (corresponding to mouse E121, Y129 and R294, respectively)—located within this area. These findings indicate that the C-terminal conserved region

likely represents a binding site for other protein partners, and the associated mutations may contribute to HCM by disrupting these interactions.

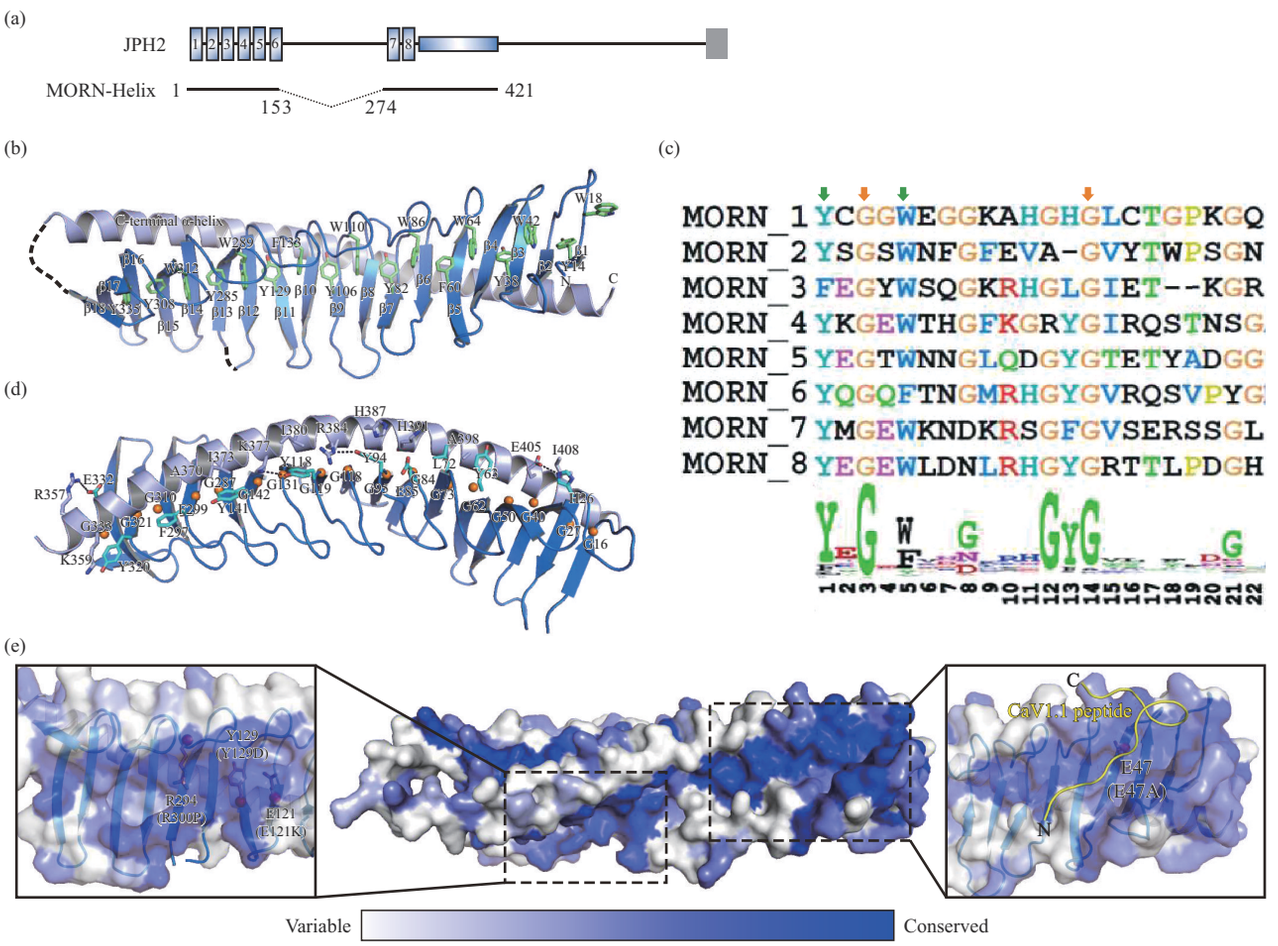

Fig. 3　Crystal structure of the JPH2 MORN−Helix domain

(a) Schematic of the crystallization construct, with the unstructured Joining region (residues 154−273) deleted to yield the JPH2 MORN-Helix domain (residues 1−153 and 274−421). (b) Ribbon diagram of the 2.6 Å JPH2 MORN-Helix structure, with key aromatic residues in the folding core highlighted as stick models. (c) Sequence alignment of MORN repeats from mouse JPH2, with a sequence logo generated from alignments of all MORN repeats in human proteins. (d) Combined ribbon and stick model illustrating interactions between the MORN repeats and the C-terminal α-helix. (e) Conservation map of JPH2, highlighting two conserved regions in the inner groove, based on sequence alignment of vertebrate JPHs. Identical residues are colored dark blue, strongly similar residues blue, weakly similar residues light blue, and variable residues white.

Concurrently with our study, Yang *et al*. [23] reported the crystal structures of human JPH1 and JPH2 MORN-Helix domains. To assess structural consistency, we compared our JPH2 MORN-Helix structure with their JPH1 and JPH2 structures, as well as with AlphaFold2-predicted models for mouse JPH2. The comparisons revealed a high degree of structural similarity across all structures (Figure S3).

2.4　Membrane binding property of the JPH2 MORN−Helix domain

MORN repeats in JPHs were initially proposed to mediate lipid membrane binding[1]. However, recent studies have challenged this view, reporting weak or negligible phospholipid interactions for some MORN motifs[23, 26-27]. To resolve this controversy, we investigated whether the JPH2 NT binds membranes and identified the sequence determinants of this interaction (Figure 4a).

We first employed a cell-based assay to assess membrane-binding properties. When GFP-tagged full-length JPH2 (GFP-JPH2 FL) was expressed in COS7 or HeLa cells, fluorescence predominantly localized

near the nucleus, consistent with endoplasmic reticulum (ER) colocalization (B1 in Figure 4b; Figure 4c, S4). In contrast, GFP-tagged JPH2 NT (residues 1−440) localized primarily to the plasma membrane, indicating robust membrane targeting (B2 in Figure 4b; Figure 4c). However, further truncations within the MORN-Helix domain—JPH2-MORN (lacking the helix) and JPH2-Helix (lacking MORN repeats) —completely abolished membrane localization (B3, B4 in Figure 4b; Figure 4c). These results suggest that the intact MORN-Helix structure is essential for membrane association.

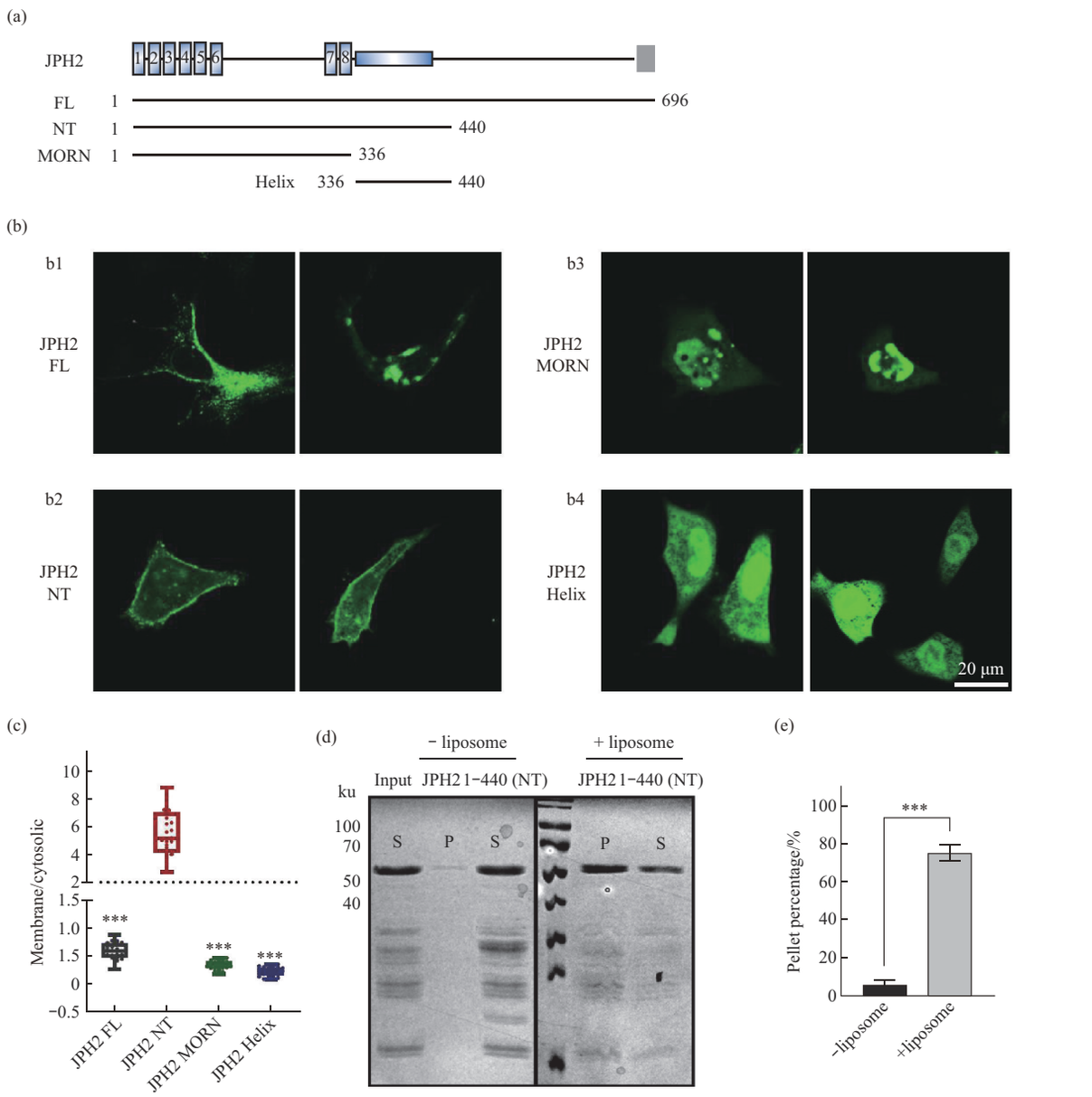

Fig. 4 JPH2 MORN−Helix domain mediates membrane localization

(a) Schematic of JPH2 constructs—full-length (FL), N-terminal (NT, residues 1−440), MORN, and Helix fragments, designed based on domain architecture and conservation patterns to evaluate membrane localization. (b) Representative confocal microscopy images of COS7 and HeLa cells expressing GFP-tagged JPH2 constructs. The JPH2 NT construct (b2) shows prominent plasma membrane localization, whereas MORN (b3) and Helix (b4) constructs exhibit markedly impaired membrane targeting. (c) Quantitative analysis of GFP fluorescence intensity ratios (membrane to cytosolic) across constructs. Data represent means±SD from >30 cells per group, analyzed by one-way ANOVA compared to the JPH2 NT group. ***P<0.001. (d) Liposome-binding assay assessing lipid-binding properties of JPH2 NT. Fractions labeled “ P ” (pellet) or “ S ” (supernatant) indicate protein distribution after centrifugation with or without liposomes. JPH2 NT directly interacts with liposomes, supporting its role in membrane association. (e) Quantification of JPH2 NT in pellet fractions from panel (d). Values are means±SD from three independent experiments, analyzed by independent-sample t-test. ***P< 0.001.

To confirm direct lipid interactions, we performed an in vitro liposome-binding assay. In the absence of liposomes, JPH2 NT remained predominantly in the supernatant (S) after ultracentrifugation. Upon addition of liposomes, over 50% of JPH2 NT co-sedimented with the liposomes, as evidenced by its presence in the pellet (P) (Figure 4d, e). These findings demonstrate that JPH2 NT directly binds lipid membranes, reinforcing the critical role of the MORN-Helix domain in mediating membrane association.

2.5 Sequence determinants of membrane binding

Electrostatic potential analysis of the JPH2 MORN-Helix structure revealed no prominent positively charged surface on the MORN repeats or the backbone α-helix that could account for membrane binding. However, detailed analysis combining multiple sequence alignment and AlphaFold2-predicted models identified a short, flexible linker segment (residues 340−358) between the eight MORN repeats and the α-helix, containing seven highly conserved positively charged residues (Arg/Lys) (Figure 5a). This segment exhibits high flexibility, as residues 343−353 were unresolved in the final electron density map of our 2.6 Å crystal structure.

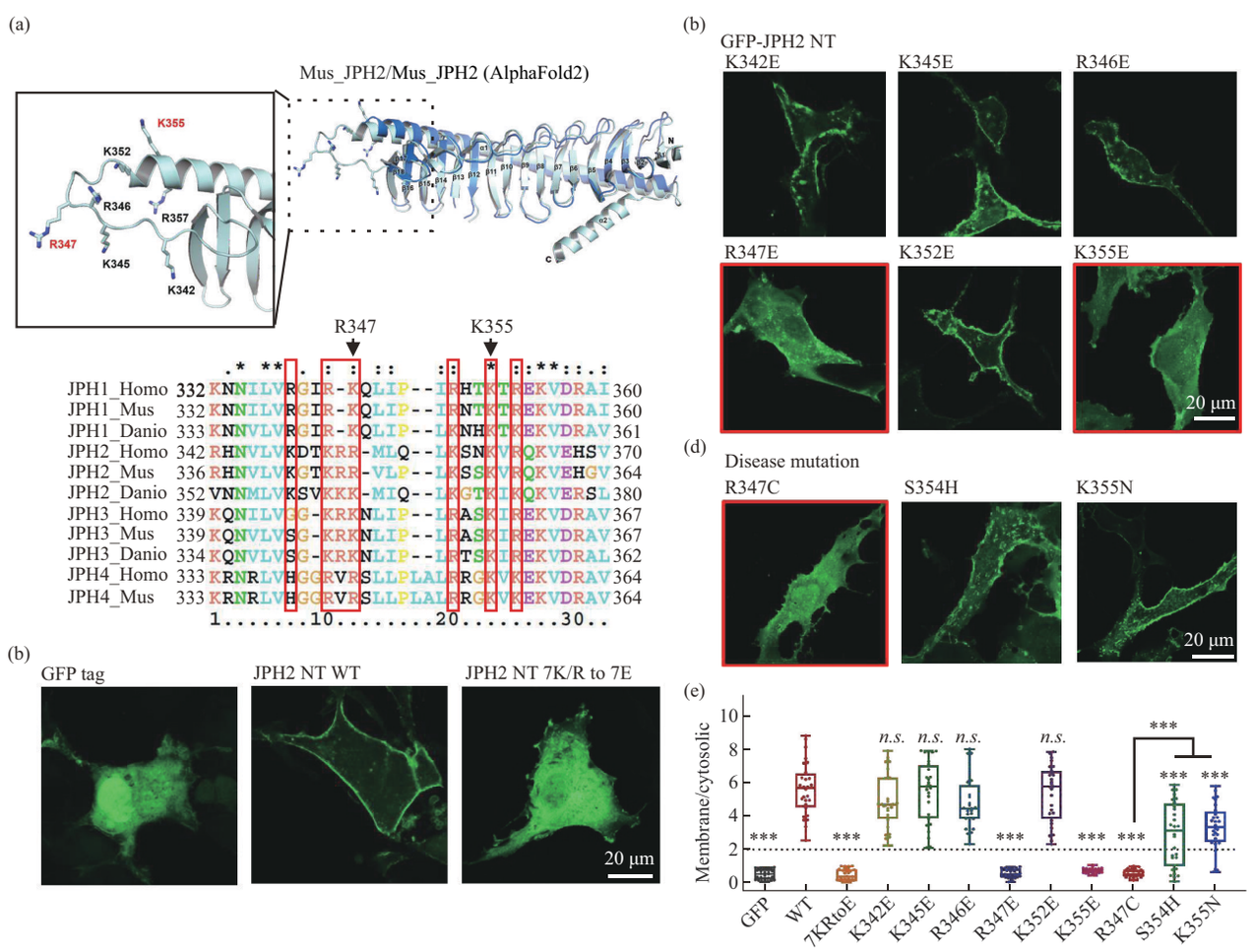

Fig. 5　R347E and R347C mutations disrupt JPH2 membrane localization

(a) Ribbon representations of the JPH2 MORN-Helix crystal structure and AlphaFold3-predicted model, highlighting a linker segment (residues 340−358) with seven positively charged residues. Sequence alignment of the linker region across species (Homo: *Homo sapiens*, Mus: *Mus musculus*, and Danio: *Danio rerio*) shows conserved residues, with red boxes marking the seven positively charged positions. (b) Representative confocal microscopy images of COS7 cells expressing wild-type (WT) and mutant forms of EGFP-tagged JPH2 NT, showing loss of plasma membrane localization upon mutation of seven conserved positively charged residues in the linker segment to glutamic acid (7K/R to 7E). (c) Representative confocal microscopy images of COS7 cells demonstrating that single mutations R347E or K355E in EGFP-JPH2 NT abolish plasma membrane localization, underscoring their critical role in membrane targeting. (d) Representative confocal microscopy images of COS7 cells revealing that the HCM-associated mutation R347C in EGFP-JPH2 NT disrupts plasma membrane localization. (e) Quantitative analysis of GFP fluorescence intensity ratios (membrane to cytosolic) across constructs. Data represent means ± SD from >30 cells per group, analyzed by one-way ANOVA compared to WT JPH2 NT. *n.s.*: not significant, ***P<0.001.

To test whether these positively charged residues mediate membrane binding, we mutated all seven to negatively charged glutamic acid (7K/R to 7E) in GFP-tagged JPH2 NT and expressed the construct in HeLa cells. Unlike the wild-type (WT) JPH2 NT, which showed strong plasma membrane localization, the 7K/R to 7E mutant displayed diffuse cytoplasmic fluorescence, indicating a complete loss of membrane targeting (Figure 5b, e). To pinpoint critical residues, we individually mutated each of the seven residues to glutamic acid. The R347E and K355E mutants exhibited diffuse fluorescence, similar to the 7K/R to 7E mutant, whereas the other single mutants retained predominantly membrane-associated fluorescence (Figure 5c, e). These results suggest that R347 and K355 are essential for membrane binding.

Notably, the linker segment harbors HCM-associated mutations, including R347C, S354H, and K355N (corresponding to human R353C, N360H, and K361N, respectively, Table S1). Strikingly, the R347C mutant, like R347E, abolished membrane localization in HeLa cells, displaying diffuse cytoplasmic fluorescence (Figure 5d, e). The S354H and K355N mutants also displayed reduced membrane localization, though their effects were less severe. These findings indicate that impaired membrane binding, particularly driven by the R347C mutation and to a lesser extent by S354H and K355N, may underlie the disease mechanism of HCM in affected individuals.

3 Discussion

Obtaining purified recombinant proteins under physiological conditions is critical for detailed biochemical studies, particularly those investigating membrane binding and protein interactions that may rely on electrostatic forces. An earlier report has described the purification of JPH1 and JPH2 MORN repeat fragments only under high-salt conditions, such as 500 mmol/L NaCl. In this study, we successfully purified a recombinant JPH2 N-terminal fragment containing MORN repeats under moderate salt concentrations using an optimized buffer with 100 mmol/L $MgSO_4$. Intriguingly, sulfate ions were observed in both our JPH2 MORN-Helix crystal structure and the reported JPH2/CaV1.1 complex structure, which might be the reason why $MgSO_4$ can stabilize the protein. This methodological advance establishes a robust foundation for subsequent interaction studies, enabling comprehensive characterization of JPH2’s functional properties.

Leveraging this purification strategy and further construct optimization, we determined the 2.6 Å crystal structure of the mouse JPH2 MORN-Helix domain, despite concurrent reports of human JPH1 and JPH2 structures. Our structure provides several key insights. First, the tight coupling between the MORN repeats and the C-terminal α-helix refutes earlier models proposing that MORN repeats solely mediate membrane binding while the α-helix serves as a spacer between plasma and ER membranes. Instead, both elements are essential for membrane association, as demonstrated by our cell-based and liposome-binding assays. Second, the structure elucidates the folding mechanism of MORN repeats, revealing a unique core of alternating aromatic residues from each β-strand, stabilized by the C-terminal α -helix, consistent with our prior MORN4 findings. However, this α-helix is not universally required for MORN repeat stability, as seen in *Trypanosoma brucei* MORN1[28], radial spoke head 1 homolog (RSPH1) [29-30], and SETD7 methyltransferase[31], which lack this feature. Finally, conservation analysis revealed that the inner groove of JPH2’s MORN repeats is highly conserved, reinforcing our previous hypothesis from MORN4 studies that MORN repeats, like ankyrin or armadillo repeats, serve as general protein-binding modules. Supporting this, recent structural studies identified the N-terminal conserved region as the CaV1.1 binding site, with the HCM-associated mutation E47A located on its surface. Similarly, the C-terminal conserved region harbors multiple HCM-related mutations (*e.g.*, E121K, Y129D, R300P) on its surface, suggesting additional protein partners may interact with JPH2’s MORN repeats. The identity of these partners and the functional impact of these mutations require further investigation.

MORN repeats typically comprise 23−26 amino acids forming a β-hairpin structure, stabilized by hydrophobic interactions between conserved aromatic residues at positions 1, 5, and 10 of each repeat. In JPH2, eight canonical MORN repeats and two capping repeats form a U-shaped groove for target binding, while MORN1-5 and SETD7 contains 2−7 MORN repeats with a similar hydrophobic pattern, suggesting a conserved folding mechanism. Glycine residues at key positions enable sharp turns and

hairpin flexibility, essential for maintaining structural integrity and ligand interaction. Despite major sequence variations, these shared structural features indicate that proteins contain MORN repeats may likewise adopt a U-shaped groove capable of engaging target proteins (Figure S2).

JPHs are known for their association with the plasma membrane, with phosphatidylserine (PS) and phosphatidylinositides (PIPs), proposed as potential ligands[24, 32]. Alternatively, palmitoylation has been suggested to enhance stable membrane anchoring[26]. However, recent studies failed to obtain JPH2 complex structures bound to PI(4, 5)P2 or PS, even under high lipid concentrations, possibly due to weak binding affinity or the reliance on high-salt conditions for JPH1/2 protein purification[23]. Our optimized purification strategy, utilizing a 100 mmol/L $MgSO_4$ buffer, enabled the purification of the JPH2 NT under near-physiological salt concentrations, facilitating robust membrane-binding studies. Indeed, our liposome-binding assays confirmed direct interactions between JPH2 NT and liposomes, and structural analysis identified a flexible linker segment containing positively charged residues which are critical for this binding. Importantly, our mutagenesis studies revealed that the HCM-associated mutation R347C specifically disrupts membrane association, highlighting the critical role of membrane binding in JPH2 function and disease pathogenesis. Unlike membrane-binding modules such as PH domains, which selectively engage specific lipid head groups *via* defined pockets, these positively charged residues in JPH2 do not form a structured pocket, suggesting non-selective electrostatic interactions drive membrane avidity. Given that JPH2’s MORN repeats also interact with membrane proteins like CaV1.1, this membrane avidity likely synergizes with protein binding to enhance JMC stability. Consistent with this, literature reports and our findings indicate that JPH2’s interaction with CaV1.1 has a moderate dissociation constant in the micromolar range[23], which alone may be insufficient for stable JMC formation. The cooperative effect of membrane avidity likely ensures robust JMC assembly.

4 Conclusion

In summary, this study provides structural insights into the membrane-binding mechanism of cardiomyocyte-specific junctophilin-2. The solved crystal structure of the JPH2 MORN-Helix domain highlights its dual functional roles: serving as both a membrane-anchoring module and a protein-interaction interface. The positively charged linker segment adjacent to the MORN motifs was identified as a critical determinant for direct membrane association through electrostatic interactions with phospholipid bilayers.

Furthermore, functional assays demonstrated that the HCM-associated R347C mutation abolishes membrane localization without disrupting the overall MORN-Helix fold, providing a mechanistic explanation for how this mutation may impair JPH2 function and contribute to disease pathogenesis. These findings resolve previous uncertainties regarding the functional significance of MORN repeats and their associated structural elements in JPH2.

Collectively, this work not only advances the molecular understanding of the JPH2’s role in cardiac excitation-contraction coupling but also establishes a structural framework for future investigations into the assembly, regulation, and pathological remodeling of JMCs in the heart. The study further underscores the importance of integrating structural and functional analyses to delineate the mechanisms by which junctophilins maintain membrane microdomains essential for physiological cardiac function and how their disruption may lead to inherited cardiomyopathies.

Acknowledgements The authors thank the staff members of BL19U1 beamlines at the National Facility for Protein Science in Shanghai (https://cstr.cn/31129.02.NFPS), for technical support in X-ray diffraction data collection and analysis.

Data availability The atomic coordinates and the structure factors of mouse JPH2 MORN-Helix structure has been deposited to the Protein Data Bank (PDB) under the accession code 9UO9 (https://rcsb.org/structure/9UO9).

Supplementary Available online (http://www.pibb.ac.cn, http://www.cnki.net):
PIBB_20250183_Figure_S1.pdf
PIBB_20250183_Figure_S2.pdf
PIBB_20250183_Figure_S3.pdf

PIBB_20250183_Figure_S4.pdf
PIBB_20250183_Table_S1.pdf

References

[1] Takeshima H, Komazaki S, Nishi M, *et al*. Junctophilins: a novel family of junctional membrane complex proteins. Mol Cell, 2000, **6**(1): 11-22

[2] Lehnart S E, Wehrens X H T. The role of junctophilin proteins in cellular function. Physiol Rev, 2022, **102**(3): 1211-1261

[3] Hall D D, Takeshima H, Song L S. Structure, function, and regulation of the junctophilin family. Annu Rev Physiol, 2024, **86**: 123-147

[4] Dixon R E, Trimmer J S. Endoplasmic reticulum-plasma membrane junctions as sites of depolarization-induced Ca^{2+} signaling in excitable cells. Annu Rev Physiol, 2023, **85**: 217-243

[5] Franzini-Armstrong C. The relationship between form and function throughout the history of excitation-contraction coupling. J Gen Physiol, 2018, **150**(2): 189-210

[6] Takei D, Takeshima H. Excitation-contraction coupling and junctional membrane structures. Clin Calcium, 2017, **27**(3): 333-338

[7] Perni S, Beam K. Junctophilins 1, 2, and 3 all support voltage-induced Ca^{2+} release despite considerable divergence. J Gen Physiol, 2022, **154**(9): e202113024

[8] Nakada T, Kashihara T, Komatsu M, *et al*. Physical interaction of junctophilin and the $Ca_V1.1$ C terminus is crucial for skeletal muscle contraction. Proc Natl Acad Sci USA, 2018, **115**(17): 4507-4512

[9] Sahu G, Wazen R M, Colarusso P, *et al*. Junctophilin proteins tether a Cav1-RyR2-$KCa_{3.1}$ tripartite complex to regulate neuronal excitability. Cell Rep, 2019, **28**(9): 2427-2442.e6

[10] Pritchard H A T, Griffin C S, Yamasaki E, *et al*. Nanoscale coupling of junctophilin-2 and ryanodine receptors regulates vascular smooth muscle cell contractility. Proc Natl Acad Sci USA, 2019, **116**(43): 21874-21881

[11] Reynolds J O, Chiang D Y, Wang W, *et al*. Junctophilin-2 is necessary for T-tubule maturation during mouse heart development. Cardiovasc Res, 2013, **100**(1): 44-53

[12] Parker L E, Kramer R J, Kaplan S, *et al*. One gene, two modes of inheritance, four diseases: a systematic review of the cardiac manifestation of pathogenic variants in JPH2-encoded junctophilin-2. Trends Cardiovasc Med, 2023, **33**(1): 1-10

[13] Takeshima H, Hoshijima M, Song L S. Ca^{2+} microdomains organized by junctophilins. Cell Calcium, 2015, **58**(4): 349-356

[14] Perni S, Lavorato M, Beam K G. *De novo* reconstitution reveals the proteins required for skeletal muscle voltage-induced Ca^{2+} release. Proc Natl Acad Sci USA, 2017, **114**(52): 13822-13827

[15] Zhou J, Liu H, Lin Y, *et al*. Membrane occupation and recognition nexus (MORN) motif controls protein localization and function. FEBS Lett, 2022, **596**(14): 1839-1850

[16] Yu F, Wang Q, Li M, *et al*. *Aquarium*: an automatic data-processing and experiment information management system for biological macromolecular crystallography beamlines. J Appl Crystallogr, 2019, **52**(2): 472-477

[17] McCoy A J, Grosse-Kunstleve R W, Adams P D, *et al*. *Phaser*crystallographic software. J Appl Crystallogr, 2007, **40**(4): 658-674

[18] Varadi M, Bertoni D, Magana P, *et al*. AlphaFold protein structure database in 2024: providing structure coverage for over 214 million protein sequences. Nucleic Acids Res, 2024, **52**(D1): D368-D375

[19] Emsley P, Lohkamp B, Scott W G, *et al*. Features and development of coot. Acta Crystallogr D Biol Crystallogr, 2010, **66**(Pt 4): 486-501

[20] Adams P D, Afonine P V, Bunkóczi G, *et al*. PHENIX: a comprehensive Python-based system for macromolecular structure solution. Acta Crystallogr D Biol Crystallogr, 2010, **66**(Pt 2): 213-221

[21] Chen V B, Bryan Arendall W, Headd J J, *et al*. MolProbity: all-atom structure validation for macromolecular crystallography. Acta Crystallogr D Biol Crystallogr, 2010, **66**(Pt 1): 12-21

[22] Abramson J, Adler J, Dunger J, *et al*. Addendum: accurate structure prediction of biomolecular interactions with AlphaFold 3. Nature, 2024, **636**(8042): E4

[23] Yang Z F, Panwar P, McFarlane C R, *et al*. Structures of the junctophilin/voltage-gated calcium channel interface reveal hot spot for cardiomyopathy mutations. Proc Natl Acad Sci USA, 2022, **119**(10): e2120416119

[24] Rossi D, Scarcella A M, Liguori E, *et al*. Molecular determinants of homo- and heteromeric interactions of Junctophilin-1 at triads in adult skeletal muscle fibers. Proc Natl Acad Sci USA, 2019, **116**(31): 15716-15724

[25] Andrew Karplus P, Diederichs K. Linking crystallographic model and data quality. Science, 2012, **336**(6084): 1030-1033

[26] Jiang M, Hu J, White F K H, *et al*. *S*-Palmitoylation of junctophilin-2 is critical for its role in tethering the sarcoplasmic reticulum to the plasma membrane. J Biol Chem, 2019, **294**(36): 13487-13501

[27] Yang Y, Valencia L A, Lu C H, *et al*. Plasma membrane curvature regulates the formation of contacts with the endoplasmic reticulum. Nat Cell Biol, 2024, **26**(11): 1878-1891

[28] Sajko S, Grishkovskaya I, Kostan J, *et al*. Structures of three MORN repeat proteins and a re-evaluation of the proposed lipid-binding properties of MORN repeats. PLoS One, 2020, **15**(12): e0242677

[29] Meng X, Xu C, Li J, *et al*. Multi-scale structures of the mammalian radial spoke and divergence of axonemal complexes in ependymal cilia. Nat Commun, 2024, **15**(1): 362

[30] Zheng W, Li F, Ding Z, *et al*. Distinct architecture and composition of mouse axonemal radial spoke head revealed by cryo-EM. Proc Natl Acad Sci USA, 2021, **118**(4): e2021180118

[31] Wilson J R, Jing C, Walker P A, *et al*. Crystal structure and functional analysis of the histone methyltransferase SET7/9. Cell, 2002, **111**(1): 105-115

[32] Bennett H J, Davenport J B, Collins R F, *et al*. Human junctophilin-2 undergoes a structural rearrangement upon binding PtdIns(3, 4, 5)P_3 and the S101R mutation identified in hypertrophic cardiomyopathy obviates this response. Biochem J, 2013, **456**(2): 205-217

Juntophilin–2膜结合及肥厚型心肌病相关突变的结构基础*

王静欣[1)] 李志炜[1)] 刘 伟[2)] 张文清[1)] 李健潮[1)**]

([1)] 华南理工大学医学院，教育部发育与疾病创新中心，广州 510006；

[2)] 深圳北京大学香港科技大学医学中心，生物医学研究所，深圳市神经结构生物学重点实验室，深圳 518036）

摘要 目的 Junctophilin-2（JPH2）是维持心肌细胞中膜连接复合物（junctional membrane complexes，JMCs）结构与功能的关键蛋白质，其N端膜占领与识别基序（membrane occupation and recognition nexus，MORN）重复序列被认为同时介导质膜锚定与蛋白质识别，但具体机制尚不明确。本研究旨在解析JPH2的膜结合分子机制，并探讨其在肥厚型心肌病中的致病潜力。**方法** 本研究优化缓冲液体系，成功在近生理条件下纯化了重组小鼠JPH2 N端片段（JPH2-NT），并采用X射线晶体学解析了其MORN-Helix结构域，获得分辨率为2.6 Å的晶体结构。结合序列保守性分析、细胞定位实验、脂质体结合实验及突变体功能测定，系统评估了JPH2-NT的膜结合特性及HCM相关突变（如R347C）对其功能的影响。**结果** 结构解析显示，JPH2 MORN-Helix结构域呈紧凑的β片层构型，核心由交替排列的芳香族氨基酸残基构成，并由C端α螺旋稳定构象。结构分析表明，MORN重复区域表面的凹槽为潜在蛋白质结合界面。功能实验发现，带正电荷的连接区驱动JPH2-NT膜结合，R347C突变显著削弱该能力，导致细胞定位异常。**结论** JPH2 MORN-Helix结构域通过连接区域介导质膜的锚定，HCM突变可通过破坏膜结合能力影响JMC稳定性。本研究为JPH2相关心肌病的致病机制提供了结构依据和功能解释。

关键词 Junctophilin-2，膜占领与识别基序重复序列，膜结合，肥厚性心肌病

中图分类号 Q51，Q71 **DOI**：10.16476/j.pibb.2025.0183 **CSTR**：32369.14.pibb.20250183

* 国家自然科学基金（32271270）资助项目。

** 通讯联系人。

Tel：15919631934，E-mail：lijch@scut.edu.cn

收稿日期：2025-04-25，接受日期：2025-06-02